

NSG-262-63

The Effects of Scattering on Small Proton Beams

W. M. Preston and A. M. Koehler

Department of Physics, Harvard University

Cambridge, Massachusetts

GPO PRICE \$ \_\_\_\_\_

CFSTI PRICE(S) \$ \_\_\_\_\_

Hard copy (HC) 2.00

Microfiche (MF) \_\_\_\_\_

ff 653 July 65

FACILITY FORM 802  
N67-27664  
(ACCESSION NUMBER)  
38  
(PAGES)  
CR-84505  
(NASA CR OR TMX OR AD NUMBER)

(THRU) 1  
(CODE) 84  
(CATEGORY)

### Abstract

The limitations due to multiple Coulomb scattering on the minimum dimensions of small collimated beams of heavy charged particles are discussed. The standard deviation  $\sigma$  for radial scattering for protons, of energies up to 160 Mev, is calculated for water and aluminum and the results compared with a number of experimental determinations. The effect of multiple scattering on the effective Bragg ionization curve is evaluated for collimated beams of circular and rectangular cross section.

1. Introduction

Small beams of high energy positive ions such as protons or alpha particles have found applications in biological research and medical therapy because of their low scattering and favorable depth dose characteristics. They have been used to create isolated, well-defined radiation lesions (for example, to destroy the pituitary gland which is located near the center of the head) with a minimum of damage to surrounding structures. Narrow rectangular "knife edge" beams have been employed as surgical tools in brain-splitting experiments or to cut the spinal cord of laboratory animals. An excellent review of the subject, with extensive bibliography, is given by Tobias.<sup>1</sup>

The present article, an outgrowth of work of the Harvard Cyclotron Biomedical Project,<sup>2</sup> deals explicitly with the effects of multiple Coulomb scattering on the dose distribution in small proton beams of energies up to about 160 Mev and evaluates the resulting limits on the minimum practical dimensions of such beams.

The results may have more general use, as for example, in calculating the minimum lateral dimensions required in designing total absorption scintillation counters and solid state detectors for measuring the energy of collimated beams of charged particles.

## 2. Calculation of the Standard Deviation for Multiple Scattering

Following initially the treatment of Bethe and Ashkin,<sup>3</sup> suppose a parallel beam of fast particles of charge  $z$ , momentum  $p$ , and velocity  $\beta c$  (where  $c$  is the velocity of light) is incident normally on a thin slab of material, thickness  $t$  g/cm<sup>2</sup>, of an element of atomic number  $Z$  and atomic weight  $A$ . If  $t$  is of such a magnitude that each particle undergoes many small-angle Coulomb scattering interactions, the emerging particles will have an approximately Gaussian angular distribution given by

$$F(\theta)d\theta = \frac{2\theta}{\sigma_\theta^2} e^{-\theta^2/\sigma_\theta^2} d\theta \quad (1)$$

where  $F(\theta)$  is the probability of a particle's emerging at an angle between  $\theta$  and  $\theta+d\theta$  with the normal and the angular standard deviation  $\sigma_\theta = \langle \theta^2 \rangle^{1/2}$ , the root mean square angular deflection.

If  $t$  is small enough so that  $p$  may be considered constant within the slab, and if the scattering angles are small,

$$\langle \theta^2 \rangle = q^2 t \text{ where } q^2 = \frac{0.314z^2}{p^2 \beta^2 c^2} \frac{Z(Z+1)}{A} \ln \left( \frac{\theta_x}{\theta_m} \right)^2 \text{ radian}^2\text{-cm}^2/\text{g} \quad (2)$$

In this,  $pc$  is in units of Mev and  $\theta_x$  and  $\theta_m$  are respectively the maximum and minimum angles of single scattering events. The value of  $\theta_m$  is determined by shielding of the nuclear charge by the atomic electrons; it may be calculated with more

than adequate precision. Except at very high energies, however, the choice of  $\theta_x$  is rather arbitrary. If we define  $\theta_x$  as that deflection which, on the average, is exceeded by only one scattering event per particle in its passage through the slab, and if the relation  $0.73Zz/\beta < 1$  holds (as it does in our present range of interest), then<sup>3</sup>

$$f = \ln(\theta_x/\theta_m) = \ln\{106z/\beta[Z^{1/3}(Z+1)t/A]^{1/2}\} \quad (3)$$

The actual scattering exceeds the Gaussian distribution at large angles. Hence a better estimate of  $\sigma_\theta^2$ , which equals  $\langle\theta^2\rangle$  only for a Gaussian distribution, is obtained by using an appropriate large-angle cut-off,  $\theta_x$ . More accurate theoretical treatments than the above are available,<sup>3</sup> but they are difficult to evaluate. It is our purpose to carry out a simplified treatment and to compare its predictions with our experimental results.

As long as  $p\beta$  varies only slightly in the thickness of the slab, we can certainly divide the latter into slices of thickness  $dx$  cm and rewrite Eq. 2 as

$$\langle\theta^2\rangle = \rho \int_0^T q^2 dx \quad (4)$$

where  $\rho$  is the density and  $T = t/\rho$  the thickness of the slab in cm. (This follows from the fact that, for small deflections, the mean square deflections  $d\langle\theta^2\rangle = pq^2dx$  are additive.)

We now make the assumption that Eq. 4 can be extended to cover the case of a slab of arbitrary thickness  $T$ , although this is a somewhat uncertain extension of the elementary theory because of the manner in which  $\theta_x$  was defined.

Referring to Fig. 1, consider the radial deviations  $r$  from the  $x$ -axis, at a distance  $S$  from the front face of a slab of thickness  $T$ , of particles whose paths coincide with the  $x$ -axis at  $x = 0$ . For small deflections, any thin layer  $dx$  will cause an increase  $d\langle r^2 \rangle$  in the mean square value  $\langle r^2 \rangle$  equal to  $(S-x)^2 d\langle \theta^2 \rangle$ . Then the radial standard deviation  $\sigma$  will be given by

$$\sigma^2 = \langle r^2 \rangle = \rho \int_0^T q^2 (S-x)^2 dx \quad \text{cm}^2 \quad (5)$$

If the initial particle range is much greater than  $T$ , the variation of  $q$  within the slab may be small enough so that we may replace  $q$  by its value  $q_c$  at the center. Convenient approximations then are

$$\langle r^2 \rangle = \rho q_c^2 S^2 T \quad \text{if } S \gg T \quad (6)$$

$$\langle r^2 \rangle = \frac{1}{3} \rho q_c^2 T^3 \quad \text{if } S = T. \quad (7)$$

In case the scattering material is a mixture, or a compound, consisting of fractions by weight  $w_i$  of atoms characterized by atomic number  $Z_i$  and atomic weight  $A_i$ , we may rewrite Eqs. 2 and 3:

$$q^2 = \frac{0.314 z^2}{\rho^2 \beta^2 c^2} F \quad (8)$$

$$F = \sum_i \frac{w_i Z_i (Z_i + 1)}{A_i} \ln \left\{ 106 z / \beta \left[ Z_i^{1/3} (Z_i + 1) \rho T / A_i \right]^{1/2} \right\} \quad (9)$$

The quantity  $F$  is a slowly varying function. It is plotted in Fig. 2 for protons in aluminum, of initial range  $\rho R_0 = 22.3 \text{ g/cm}^2$ , initial energy  $E_0 = 158 \text{ Mev}$ , and for a thickness  $T = R_0 \text{ cm}$ . (Ranges have been taken from Report No. 39, Nuclear Science Series, National Academy of Sciences Pub. No. 1133(1964)). In this case,  $F$  in Eq. 9 is a function only of  $\beta$ , whose values as a function of the depth in the scattering material,  $\rho x$ , can be computed from range-energy tables. While  $F$  becomes infinite logarithmically at the end of the proton range,  $x = R_0$ , its average value over its range is rather closely approximated by its value at midpoint,  $X = T/2$ , call it  $F(1/2T)$ .

Substituting Eq. 8 in Eq. 5 and removing  $F$  from the integral:

$$\sigma^2 = \langle r^2 \rangle \approx 0.314 z^2 \rho F(1/2T) \int_0^T \frac{(S-x)^2}{\rho^2 \beta^2 c^2} dx \text{ cm}^2 \quad (10)$$

An excellent approximate relation giving  $\rho \beta c$  as a function of the residual proton range is

$$\rho^2 \beta^2 c^2 = a(\rho R)^b = a \rho^b (R_0 - x)^b \quad (11)$$

in which  $a$  and  $b$  are constants. [If fitted at 80 and 150 Mev,  $a = 4141$  and  $b = 1.072$  for protons in water;  $a = 2992$  and  $b = 1.084$  in aluminum;  $\rho R$  in  $\text{g/cm}^2$  and  $\rho \beta c$  in Mev.]

For the special case when  $\sigma^2$  is to be calculated at a depth in material equal to the initial proton range,  $S = R_0 = T$ . Substituting Eq. 11 in 10 and integrating:

$$\sigma_o^2 = 0.314z^2 \rho^{(1-b)} F(1/2R_o) \frac{R_o^{(3-b)}}{a(3-b)} \text{ cm}^2 \text{ for } T = S = R_o \quad (12)$$

$$\sigma_o = 6.27 \times 10^{-3} [F(1/2R_o)]^{1/2} R_o^{0.954} \text{ cm (protons in water)} \quad (12a)$$

$$\sigma_o = 7.10 \times 10^{-3} [F(1/2R_o)]^{1/2} R_o^{0.958} \text{ cm (protons in aluminum)} \quad (12b)$$

Eqs. 12a and 12b are plotted in Fig. 3, (Values of  $F(1/2R_o)$  are calculated from Eq. 9, with  $T = R_o$  and  $\beta$  computed at  $x = 1/2R_o$ .) These relations are so nearly linear that the empirical equations below are just about as accurate:

$$\sigma_o = 0.0307 R_o \text{ cm (protons in water)} \quad (12c)$$

$$\sigma_o = 0.045 R_o \text{ cm (protons in aluminum)} \quad (12d)$$

If instead of Eq. 11 we substitute in Eq. 10 the somewhat less accurate relation

$$\rho^2 \beta^2 c^2 = A(\rho R) = A\rho(R_o - x) \quad (13)$$

with the single adjustable constant A, the result can readily be integrated for the case  $S = T \leq R_o$  (Referring to Fig. 1, this corresponds to finding  $\sigma$  at any depth T in the scattering material less than  $R_o$ .)

$$\sigma^2 = \frac{0.314z^2}{A} F(1/2T) \int_0^T \frac{(T-x)^2}{(R_o-x)} dx$$

$$\sigma^2 = \frac{0.314z^2}{A} F(1/2T) R_o^2 \left\{ (1-y)^2 \ln \frac{1}{1-y} + y \left( \frac{3}{2}y - 1 \right) \right\} \quad (14)$$

where  $y = T/R_o$ . At the end of the proton range,  $T = R_o$  and

Eq. (14) reduces to  $\sigma_o^2 = \frac{0.314z^2}{A} F(1/2T)R_o^2/2$ , a somewhat less accurate expression than Eq. 12. However, the relation

$$\sigma/\sigma_o = \left[ 2(1-y)^2 \ln \frac{1}{1-y} + 3y^2 - 2y \right]^{1/2} \quad (15)$$

which is plotted in Fig. 4, can be used to estimate  $\sigma$  at any value  $y = T/R_o$  in terms of  $\sigma_o$  given by Eq. 12 or Fig. 3.

(A small error is introduced by ignoring the variation in  $F(1/2T)$ .)

### 3. Beams of Circular Cross section

Consider a circular beam of particles, parallel to the x-axis and of negligible cross section, *incident* normally on a scattering medium at  $x = 0$ . After penetration to a depth  $x$  cm, at which the standard deviation (std. dev.) is  $\sigma$ , the radial intensity distribution will be

$$I(r,x) = \frac{1}{\pi\sigma^2} e^{-r^2/\sigma^2} \quad (16)$$

where  $r$  is the distance measured normal to the x-axis, and  $I$  is a function of  $x$  through the standard deviation  $\sigma(x)$ .

If we change to a variable  $u = r/\sigma$ , the fraction of the total beam flux within a circle of radius  $r = u\sigma$  is

$$F(u) = \int_0^r 2\pi r I dr = 2 \int_0^u u e^{-u^2} du = 1 - e^{-u^2} \quad (17)$$

A useful relation which follows from Eqs. (16) and (17) is that the ratio of the intensity of the beam on the perimeter of a circle of radius  $u$  to the intensity on the axis is equal

to the fraction of the total beam scattered outside of the circle, i.e.,

$$I(u)/I(o) = 1 - F(u) \quad (18)$$

If the initial beam had an appreciable cross section, with a radial intensity distribution characterized by a std. dev.  $\sigma_1$  at  $x = 0$ , the effective std. dev. at a depth  $x$  will be

$$\sigma_e^2 = \sigma^2(x) + \sigma_1^2 \quad (19)$$

Next consider a beam of finite cross section which at  $x = 0$  has passed through a circular collimator of radius  $r_c$  over which the intensity is uniform. Assuming the beam has initially negligible angular divergence, then at a depth such that  $\sigma(x) \geq r_c$  the beam will have lost its sharp edges and  $I(r)$  will approximate a Gaussian distribution with an effective std. dev. given by

$$\sigma_e^2 \approx \sigma^2(x) + r_c^2 \quad (20)$$

In this last case, that of an initially uniform beam of radius  $r_c$ , the general intensity function  $I(r,x)$  is complicated. However, the intensity  $I(o,x)$  on the axis ( $r = 0$ ) and at a depth  $x$  is easy to find. Referring to Fig. 5, the contribution to  $I(o,x)$  coming from particles which passed through a ring at  $x = 0$ , in the plane of the collimator and of area  $2\pi r dr$ , is proportional to  $2\pi r e^{-r^2/\sigma^2} dr$ , and so

$$I(o,x) = \frac{1}{\pi\sigma^2} \int_0^{r_c} 2\pi r e^{-r^2/\sigma^2} dr = 1 - e^{-r_c^2/\sigma^2} \quad (21)$$

At  $x = 0$ ,  $\sigma(x) = 0$  and hence Eq. (21) has been normalized to make  $I(0,0) = 1$ .

For a uniform beam of protons of initial range  $R_0 = 12$  cm of water, parallel to the  $x$ -axis and incident on a circular collimator of radius  $r_c$  cm, the plots of Eq. (21) in Fig. 6 show the decrease in the relative number of particles per unit area, on the axis, as a function of the water path beyond the collimator. We have here neglected absorption. The std. dev.  $\sigma(x)$  has been taken from Figs. 3 and 4.

Actually, the number of primary particles in a high energy proton beam decreases somewhat with penetration into a medium as a result of nuclear interactions. At the same time, the average linear density of ionization increases along the paths of the individual protons as their velocities decrease, rising to a maximum, the Bragg peak, near the end of the range of the beam. The "dose", in terms of the average energy absorbed per gram, varies as a result of all three factors: scattering, absorption, and changing rate of energy loss.

In Fig. 7 is plotted the relative dose  $D(0,x)$  on the axis of a circular proton beam of initial radius  $r_c$  and range  $R_0 = 12$  cm of water. The effects of scattering are negligible for a beam of sufficiently large radius, i.e., when  $r_c \gg \sigma$ . The top curve in Fig. 7 accordingly shows the variation in dose due solely to absorption and to the changing rate of energy loss. The lower curves show the effects of decreasing the collimator radius. They are obtained by multiplying the top curve, point by point, by the ordinates of the curves in Fig. 6.

#### 4. Beams of Rectangular Cross Section

Consider a beam, initially parallel to the x-axis, formed by a collimator located at  $x = 0$  of width  $w$  and effectively infinite length. Referring to Fig. 8, let P be a point in the y,z plane at a depth x in a medium at which the std. dev. is  $\sigma(x)$ . Let  $a$  be the distance of P from the center line AA' of the beam. Then the contribution to the intensity I at P due to particles which at  $x = 0$  passed through an area  $dy dz$  of the collimator will be proportional to  $e^{-r^2/\sigma^2} dy dz$  where  $r^2 = y^2 + z^2$ .

$$\begin{aligned} I(a,x) &= \frac{1}{\pi\sigma^2} \int_{-\infty}^{\infty} e^{-z^2/\sigma^2} dz \int_{a-w/2}^{a+w/2} e^{-y^2/\sigma^2} dy \\ &= \frac{1}{\sigma\sqrt{\pi}} \int_{a-w/2}^{a+w/2} e^{-y^2/\sigma^2} dy \end{aligned} \quad (22)$$

By the substitutions  $\Phi_1 = \frac{\sqrt{2}}{\sigma}(a+w/2)$  and  $\Phi_2 = \frac{\sqrt{2}}{\sigma}(a-w/2)$  Eq. 22 may be written in the form tabulated for the normal error function:

$$I(a,x) = \frac{1}{\sqrt{2\pi}} \left\{ \int_0^{\Phi_1} e^{-\Phi_1^2/2} d\Phi_1 - \int_0^{\Phi_2} e^{-\Phi_2^2/2} d\Phi_2 \right\} \quad (23)$$

which is normalized to make I approach unity as  $w \rightarrow \infty$ .

In the special case in which  $w/\sigma \ll 1$ , Eq. (22) reduces to

$$I(a,x) = \frac{1}{\sqrt{\pi}\sigma} e^{-a^2/\sigma^2} \quad (24)$$

The intensity  $I(o,x)$  on the axis ( $y = z = 0$ ) of an initially uniform, parallel beam formed at  $x = 0$  by a rectangular collimator of width  $w$  and length  $v$ , is

$$I(o,x) = \frac{1}{\pi\sigma^2} \int_{-v/2}^{v/2} e^{-z^2/\sigma^2} dz \int_{-w/2}^{w/2} e^{-y^2/\sigma^2} dy$$

which, if put in the usual tabulated form, becomes

$$I(o,x) = 4 \left( \frac{1}{\sqrt{2\pi}} \int_0^{\Phi_1} e^{-\Phi_1^2/2} d\Phi_1 \right) \left( \frac{1}{\sqrt{2\pi}} \int_0^{\Phi_2} e^{-\Phi_2^2/2} d\Phi_2 \right) \quad (25)$$

where  $\Phi_1 = v/\sqrt{2}\sigma$  and  $\Phi_2 = w/\sqrt{2}\sigma$ .

Fig. 9 shows a plot of  $I(o,x)$  as a function of  $\Phi_2 = w/\sqrt{2}\sigma$  for the case of a rectangular collimator of length much greater than its width, i.e.  $v \gg w$ .

Fig. 10 shows plots of  $I(o,x)$ , again for  $v \gg w$ , for the case of a proton beam of initial range  $R_0 = 12$  cm water, as a function of  $x$ .

Fig. 11 is a plot of the relative dose function  $D(o,x)$  on the axis of the same beam, of  $R_0 = 12$  cm and  $v \gg w$ . The top curve, as in Fig. 6, is the Bragg curve for a beam of infinite cross section; the lower curves are for various finite values of the slit width  $w$ .

## 5. Infinite Straight Edge

Suppose an initially uniform beam of protons, parallel to the  $x$  axis, strikes a collimator consisting of a single, infinite straight edge, coincident with the  $z$ -axis, at  $x = 0$ , and then enters a scattering medium. If the std. dev. is

$\sigma(x)$  at a depth  $x$ , the intensity resulting from scattering alone at a distance  $a$  from the geometrical shadow will be

$$I(a,x) = \frac{1}{2} \pm \frac{1}{\sqrt{2\pi}} \int_0^\Psi e^{-\Phi^2/2} d\Phi \quad (26)$$

where the + sign is to be used for a point  $a$  cm outside the geometrical shadow and the - sign for a point inside, and  $\Phi = \sqrt{2} a/\sigma$ .

## 6. Experimental Test of Theory

Intensity distributions of proton beams at various depths in absorbers of aluminum and water have been measured. The experimental arrangement is shown in Fig. 12. Protons of approximately 158 MeV energy from the Harvard cyclotron are degraded to a lower energy as required by the degrader, F. A narrow beam is defined by 2 mm diameter apertures in 3.8 cm thick brass plates at A and C. A thin-walled ionization chamber, IC, placed after a 7 mm diameter aperture at B, monitors the intensity of the transmitted beam. The collimated beam enters the absorber of thickness T, and the intensity distribution of the beam as it emerges from the absorber is measured by the detector, D. The detector, consisting of a small silicon diode, can be moved across the exit face of the absorber by means of a modified microscope stage equipped with remote controls and readout. The short-circuit current generated by the diode when exposed to the proton beam is integrated with respect to time using a vibrating-reed electrometer\*. The performance of this detector system is described

\*Gary Model 31 CV, Applied Physics Corp. Monrovia, Calif.

in Ref. (4). The signal from the monitor IC is fed into an integrating electrometer, and the beam is automatically switched off when a preset quantity of charge has been collected. At each position of the detector the charge collected from the silicon diode per unit charge from the IC is recorded, thus normalizing against changes in incident beam current.

A representative set of measurements for 127 MeV protons incident on water is plotted in Fig. 13. Profiles were first made at right angles to the ones shown to determine as nearly as possible the position of the true diameter. The same measurements have been re-plotted on a Gaussian scale in Fig. 14.<sup>5</sup> It is evident that the measured distributions are nearly Gaussian in form. The measured standard deviation  $\sigma_m$  is taken as one half the diameter between points of 37% relative intensity and can easily be determined from the Gaussian plots.

The width of the beam in the absence of scattering material must be taken into account. We have measured the standard deviation  $\sigma_a$  of the beam intensity distribution in air for each energy used and at several distances T. Linear interpolation was used to estimate  $\sigma_a$  at other values of T. These values were used to calculate the standard deviation due to scattering,  $\sigma$ , using the relationship

$$\sigma^2 = \sigma_m^2 - \sigma_a^2 \quad (27)$$

The results are given in Fig. 15 and Table I. Figure 16 illustrates the relationship between the standard deviations of Eq. (27) as a function of depth in the absorbers, based on the data of Figs. 13 and 14.

The uncertainty in the measured standard deviations  $\sigma_m$  and  $\sigma_a$  is estimated to be  $\pm 0.07$  mm. From Eq. (27) it follows that the error in  $\sigma$  is given approximately by

$$\epsilon = \frac{0.07}{\sigma} (\sigma_m^2 + \sigma_a^2)^{1/2} \quad (28)$$

Values of  $\epsilon$  calculated by Eq. (28) are included in Table I.

Finally, all the experimentally determined values of  $\sigma$  have been combined in Fig. 17 using the dimensionless quantities  $\sigma/\sigma_{R_0}$  and  $T/R_0$ , where  $R_0$  is the mean proton range in the scattering material and  $\sigma_{R_0}$  is the standard deviation due to scattering at the end of range. Agreement between the experimental points and the curve calculated from Eqs. (12) and (15) is reasonably good.

The intensity distribution in a beam defined by a slit of 0.75 mm width using protons of about 134 MeV incident on a water absorber was also measured. The standard deviation obtained at 11.4 cm depth is 3.68 mm while the calculated value is 3.69 mm.

The authors are happy to acknowledge the help given by Mr. Gerry Polucci, Mr. Jon Dickinson, and Mrs. Cicily Hajek.

### References

1. C. A. Tobias, "The use of accelerated heavy particles for production of radiolesions and stimulation in the nervous system", in Response of the Nervous System to Ionizing Radiation, T. J. Haley and R. S. Snider (eds.), Academic Press, New York, 1962, pp. 325-343.
2. R. N. Kjellberg, A. M. Koehler, W. M. Preston, and W. H. Sweet, "Intercranial lesions made by the Bragg peak of a proton beam", Response of the Nervous System to Ionizing Radiation, T. J. Haley and R. S. Snider (eds.) Little, Brown and Co., Boston, 1964, pp. 36-53.
3. H. A. Bethe and J. Ashkin, "Passage of radiations through matter", in Experimental Nuclear Physics, E. Segre (ed.), Wiley, New York, 1953; Part II, page 283 et seq.
4. A. M. Koehler "Dosimetry of proton beams using small silicon diodes", **Conf. on space radiation biology, Berkeley, Calif. Sept. 7 - 10, 1965.**
5. Peter Onno, "New graph paper for the analysis of Gaussian distributions," Rev. Sci. Instr. 32, 1253 (1961).

TABLE I

Material	$E_0$ (MeV)	$R_0$ (cm)	T (cm)	$\sigma_m$ (mm)	$\sigma_a$ (mm)	Experimental $\sigma \pm \epsilon$ (mm)	Calculated $\sigma$ (mm)
Air	158		0.63	1.35	1.35		
"	"		8.25	1.45	1.45		
Aluminum	"	8.25	2.54	1.42	(1.38) (a)	0.35	0.52
"	"	"	5.08	2.15	(1.41)	1.62	1.64
"	"	"	6.35	2.75	(1.43)	2.35	2.34
"	"	"	7.62	3.55	(1.44)	3.24	3.20
"	"	"	8.25	3.72	1.45	3.43	3.72
Air	127		0.2	1.35	1.35		
"	"		11.0	1.68	1.68		
Water	"	11.4	5.7	1.90	(1.51)	1.15	1.08
"	"	"	8.7	2.70	(1.60)	2.18	2.17
"	"	"	11.4	3.85	(1.68)	3.46	3.50
Air	112		0.63	1.40	1.40		
Aluminum	"	4.44	2.54	1.72	(1.42)	0.97	0.79
"	"	"	3.81	2.20	(1.44)	1.66	1.54
"	"	"	4.44	2.52	(1.45)	2.06	2.02
Water	134	12.8	12.4	3.8	(0.94)	3.68	3.69

(a) Figures in parentheses are interpolated values; see text.

Figure Captions

1. A scattering event in an element  $dx$ , at a distance  $x$  from the front face of a slab of material of total thickness  $T$ , causes a displacement  $r$  in the position of a particle, measured at a distance  $S$  from  $x = 0$ .
2. The function  $F(px)$ , defined by Eq. 9, for protons of initial range  $R_0 = 2.33 \text{ g/cm}^2$  in aluminum.
3. Values of  $\sigma_0$ , the standard deviation for protons of initial range  $R_0 \text{ g/cm}^2$ , at the end of their range, calculated from Eqs. 12a and 12b for water and aluminum respectively.
4. The calculated ratio  $\sigma/\sigma_0$  of the standard deviation for protons, of initial range  $R_0$ , at a depth  $T$  in a given material, to that at the end of the proton range.
5. A parallel beam of particles is initially limited by a circular collimator of radius  $r_c$ .
6.  $I(0,x)$  is the calculated relative intensity (protons/cm<sup>2</sup>) on the axis of a uniform circular beam, of initial range  $R_0 = 12 \text{ cm}$  of water and radius  $r_c \text{ mm}$  at the collimator, as a function of water path  $x$ . Absorption is neglected; the change is due to scattering alone.
7. The relative dose  $D(0,x)$  on the axis of a uniform circular proton beam, of initial range  $R_0 = 12 \text{ cm}$  of water and radius  $r_c \text{ mm}$  at the collimator, as a function of water path  $x$ . The curve for  $r_c = \infty$  is an experimental Bragg curve, the others are calculated.

Figure Captions (continued)

8. Scattering to a point P, at a distance  $a$  from the axis AA' of a collimated rectangular beam of width W, from an element  $dx dy$ .
9. The function  $I(o,x)$  of Equation 25, plotted vs.  $\Phi_2 = W\sqrt{2}\sigma$ , where W is the width of a rectangular collimator, of length  $V \gg W$ ;  $\sigma$  is the std. dev. for scattering, and  $I(o,x)$  is the intensity on the axis at a depth x.
10. The calculated intensity  $I(o,x)$ , on the axis at a depth x, for a proton beam from a rectangular collimator, of width W mm and length  $V \gg W$ , and initial range  $R_0 = 12$  cm of water. Absorption is neglected.
11. Relative dose  $D(o,x)$  on the long axis of a uniform rectangular beam, of initial range  $R_0 = 12$  cm of water, width W, and length  $V \gg W$ , as a function of water path x. The curve  $W = \infty$  is an experimental Bragg curve, the others are calculated.
12. Diagram of experimental arrangement. The proton beam is incident on the degrader, F, and is collimated by 2 mm diameter apertures at A and C. The ion chamber IC behind a 7 mm aperture at B monitors the transmitted beam. The absorber of thickness T is placed about 20 cm after C. The silicon diode detector at D measures intensity as a function of position y along a diameter.

Figure Captions (continued)

13. Beam intensity as a function of position along a diameter of the beam, measured at 0 cm (a), 5.7 cm (b), 8.7 cm (c), and 11.4 cm (d) depth of penetration in water. The incident energy is 127 MeV and the mean end of range is at 11.4 cm depth.
14. Data of Figure 13 normalized to 100% intensity at maximum and plotted on a Gaussian scale.
15. The standard deviation due to scattering at various depths. The curves are calculated from Eqs. (12) and (15) of Section 2, while the points are experimental results. Curve (a) is for 112 MeV protons on aluminum, curve (b) is for 158 MeV protons on aluminum, and curve (c) is for 127 MeV protons on water.
16. The relationship between beam-width in the absence of scattering,  $\sigma_0$ ; the scattering contribution,  $\sigma$ ; and the total observed width  $\sigma_m$ . The data of Figures 13 and 14 have been used for this example.
17. Dimensionless plot of the standard deviation due to scattering versus depth of penetration. The curve is a plot of Eq. (15) of Section 2. Open triangles are experimental results for 112 MeV protons on aluminum; solid triangles for 158 MeV protons on aluminum; open circles for 127 MeV protons on water.

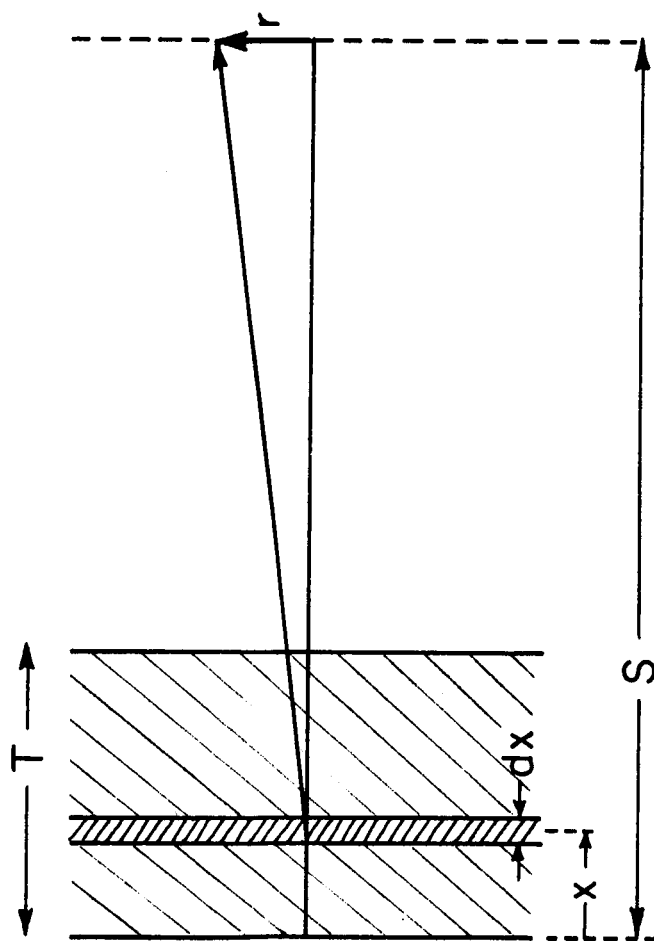


FIGURE I

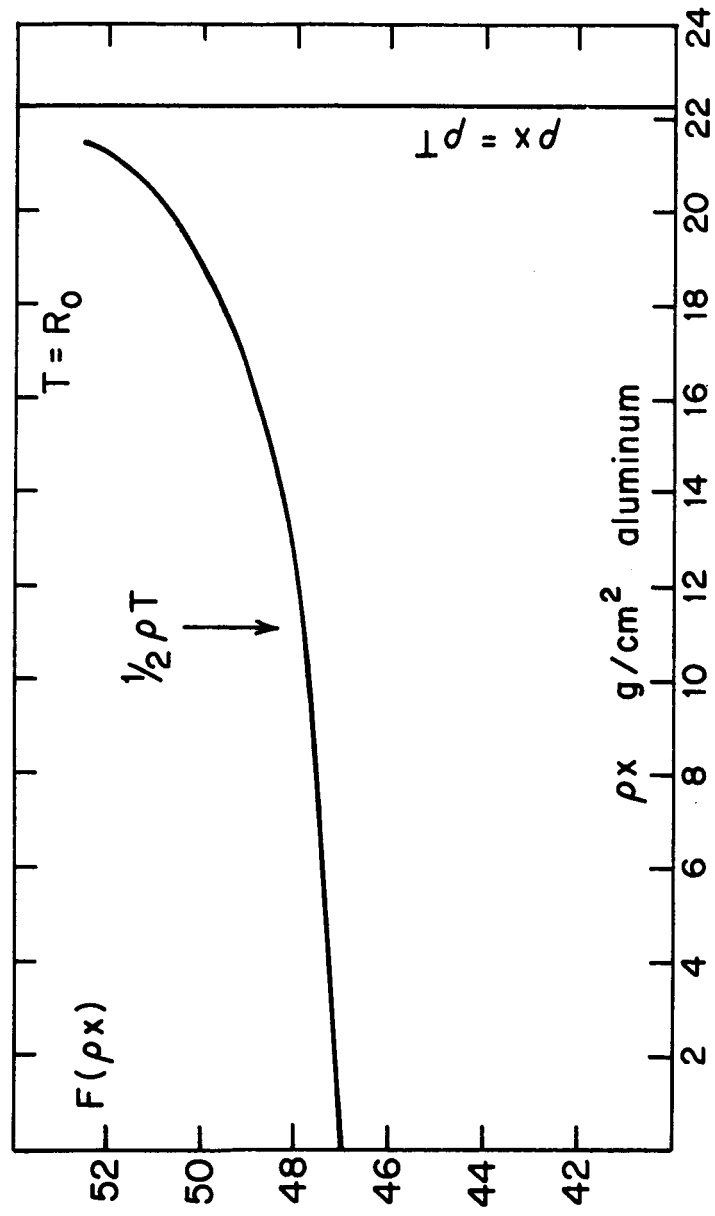


FIGURE 2

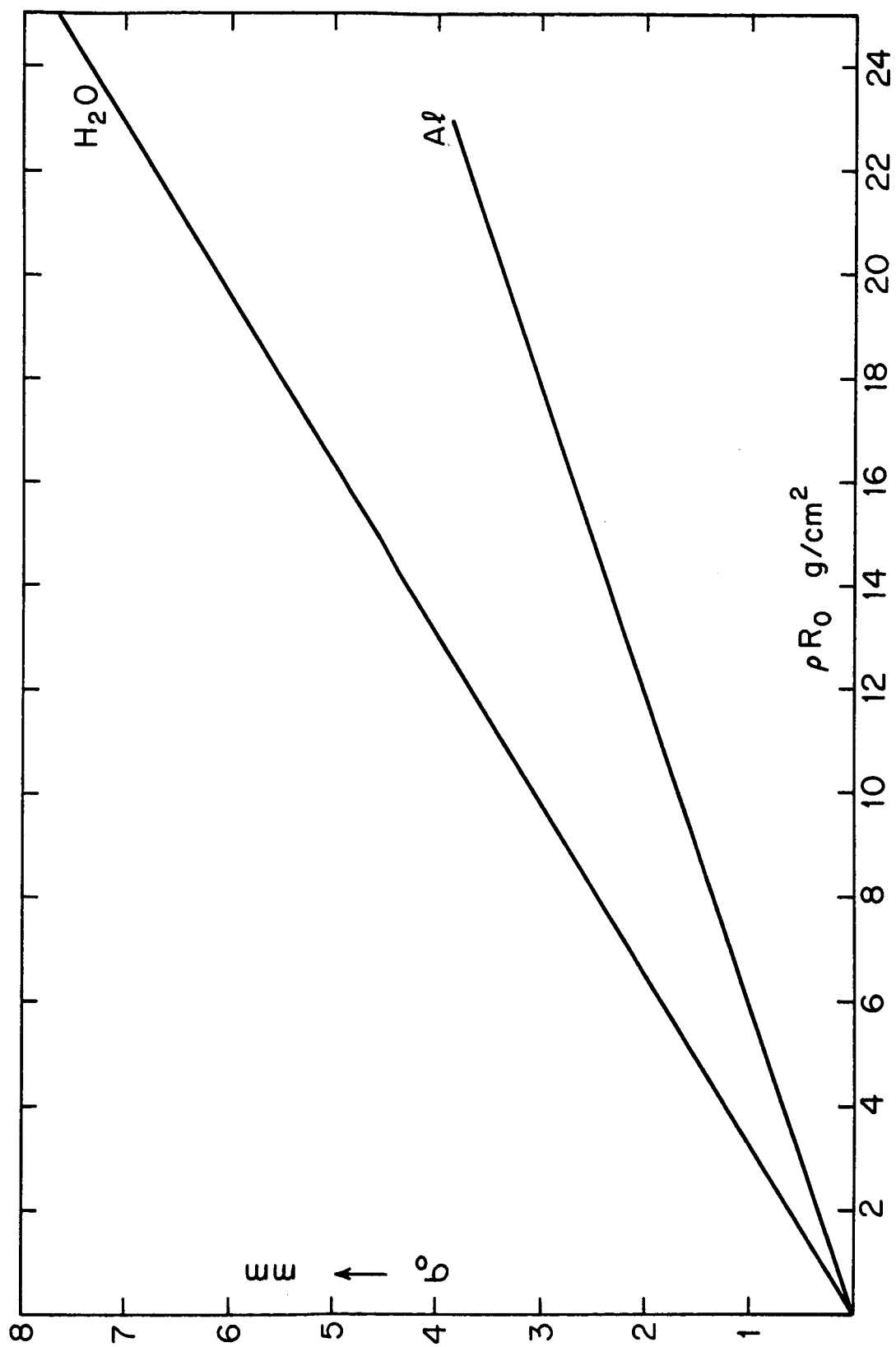


FIGURE 3

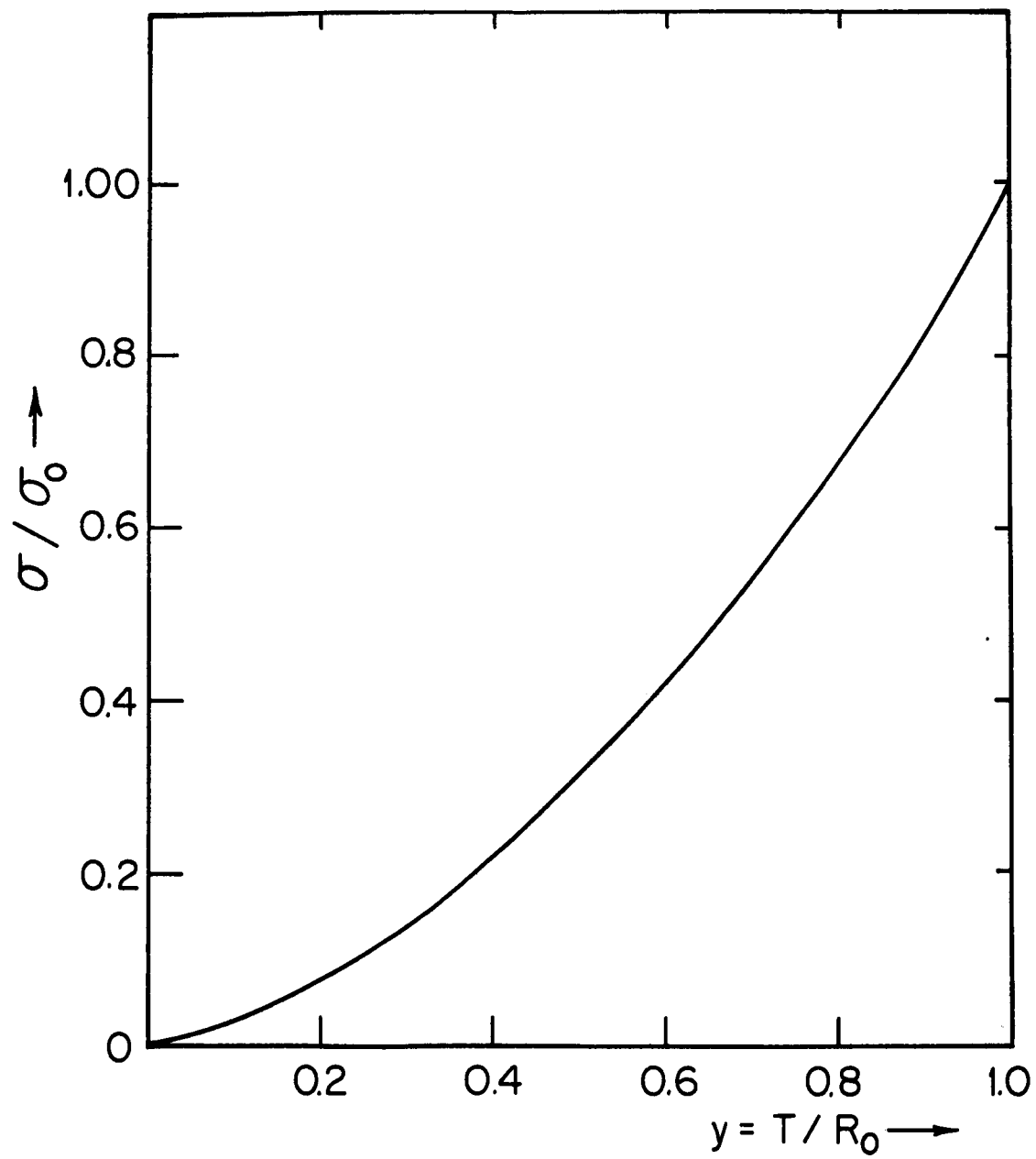


FIGURE 4

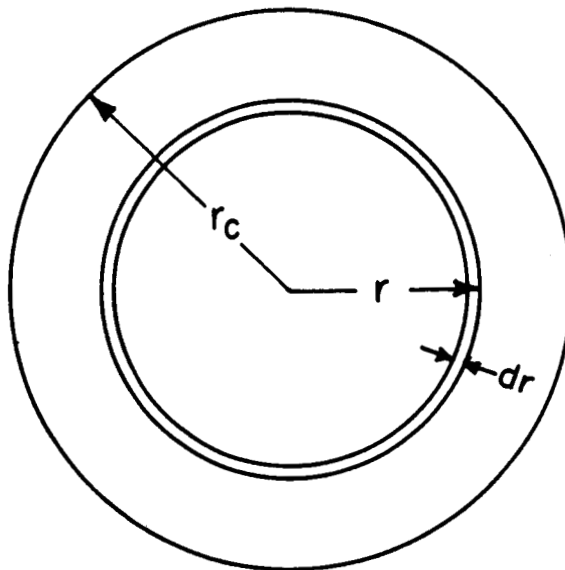


FIGURE 5

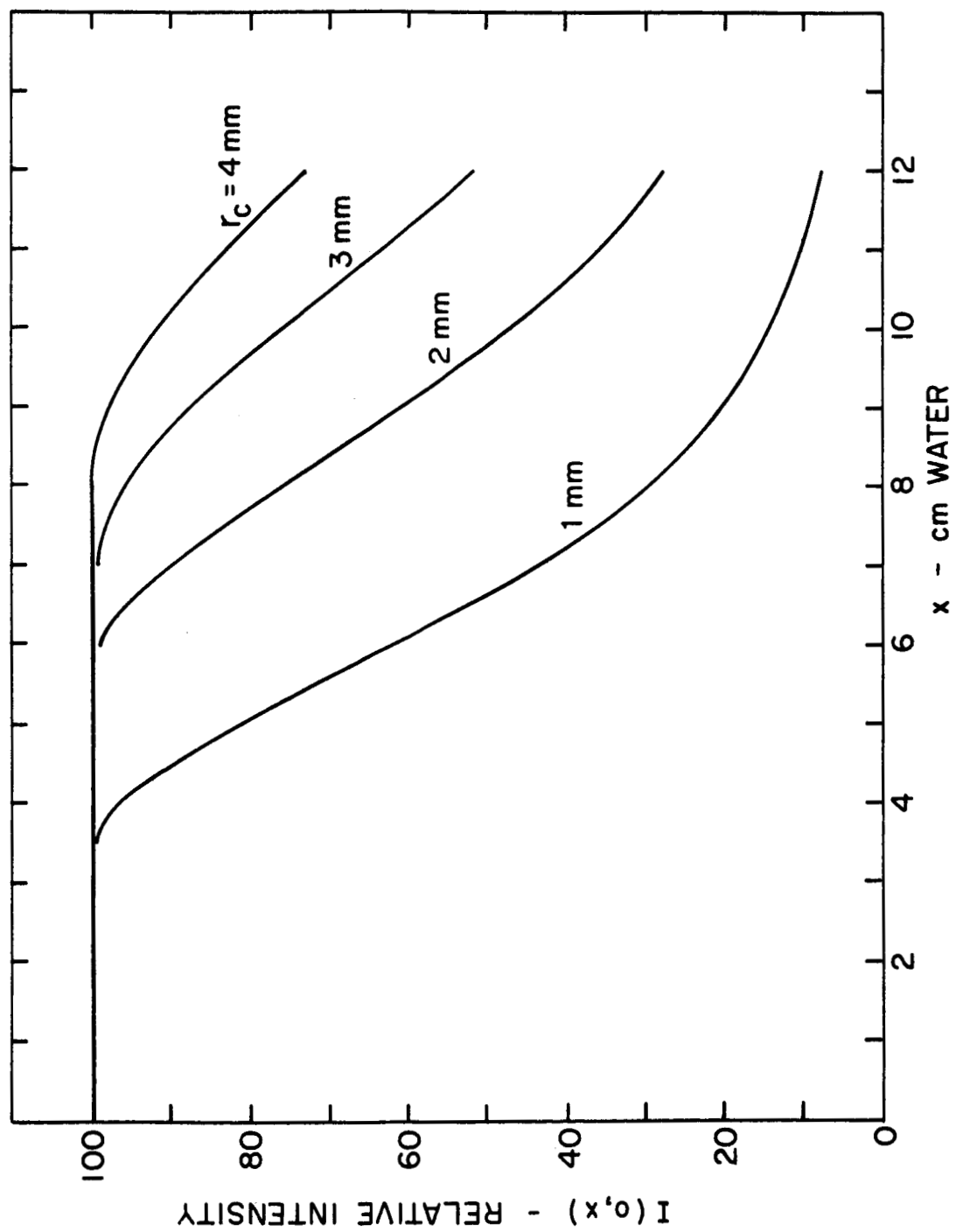


FIGURE 6

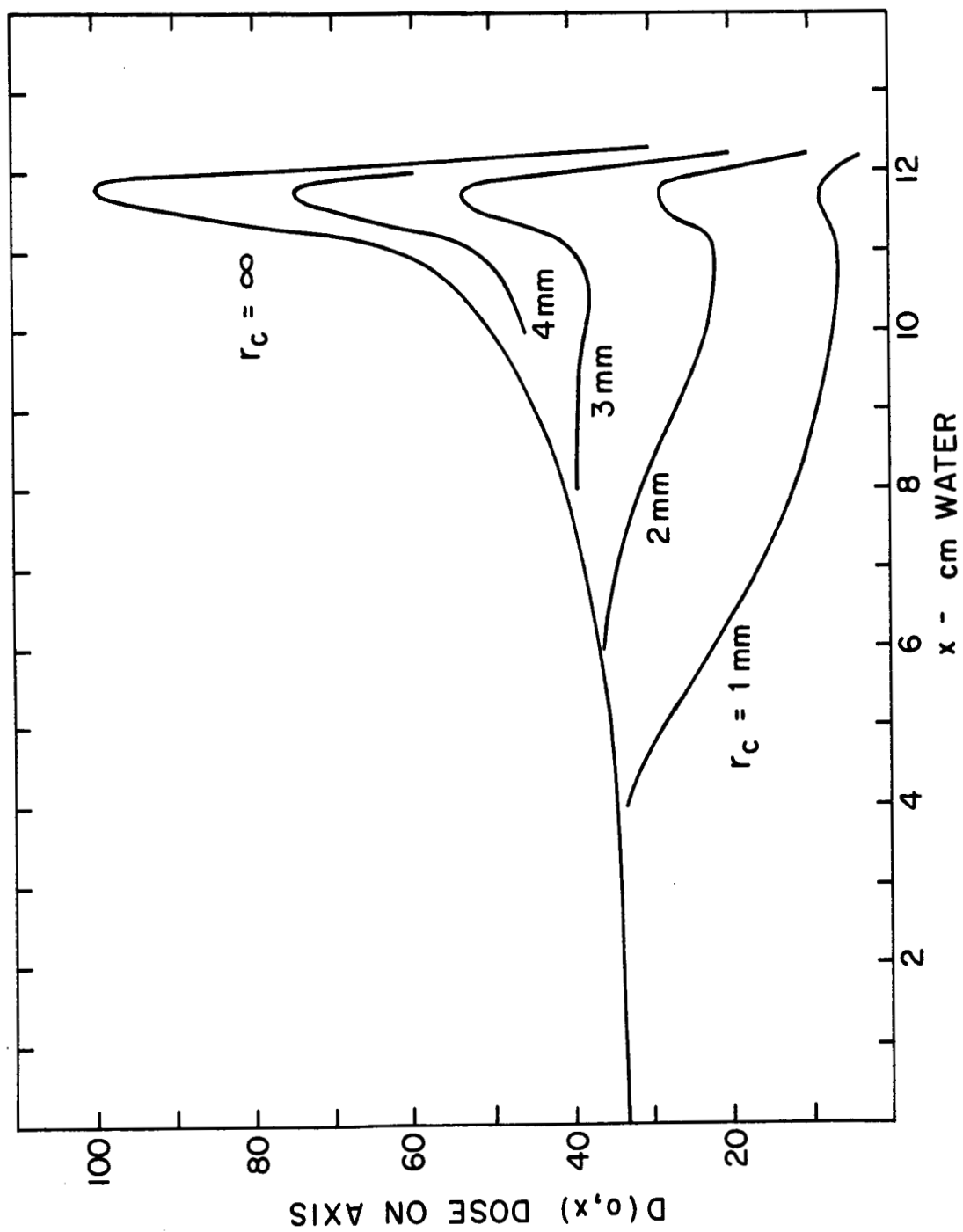


FIGURE 7

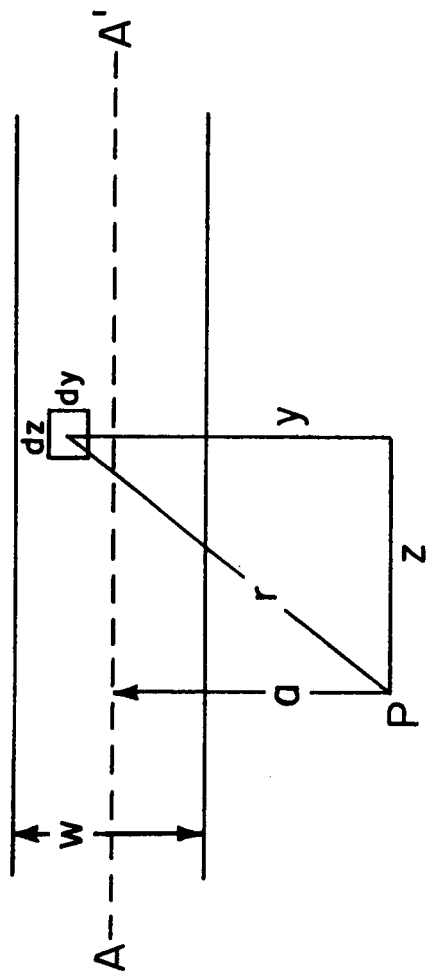


FIGURE 8

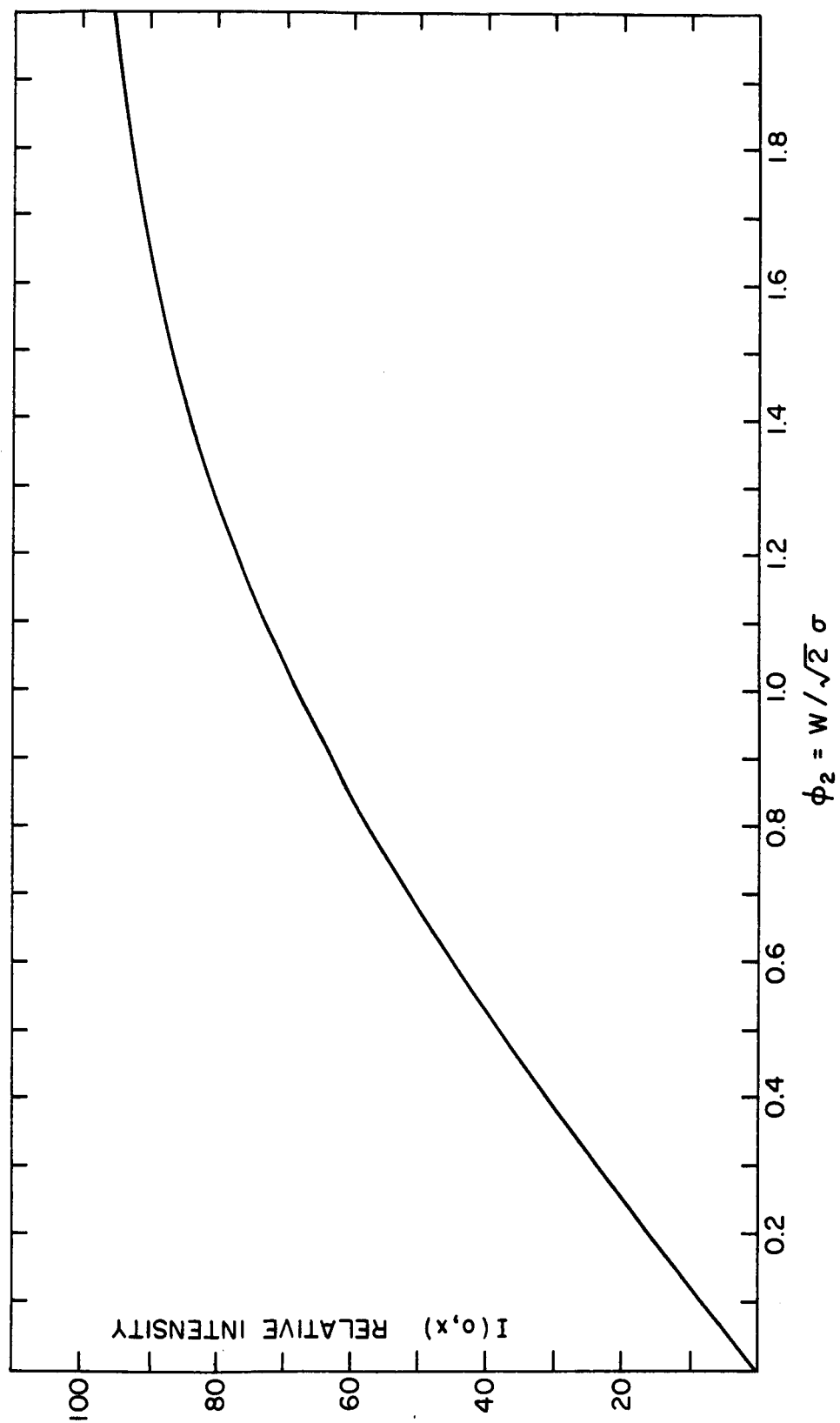


FIGURE 9

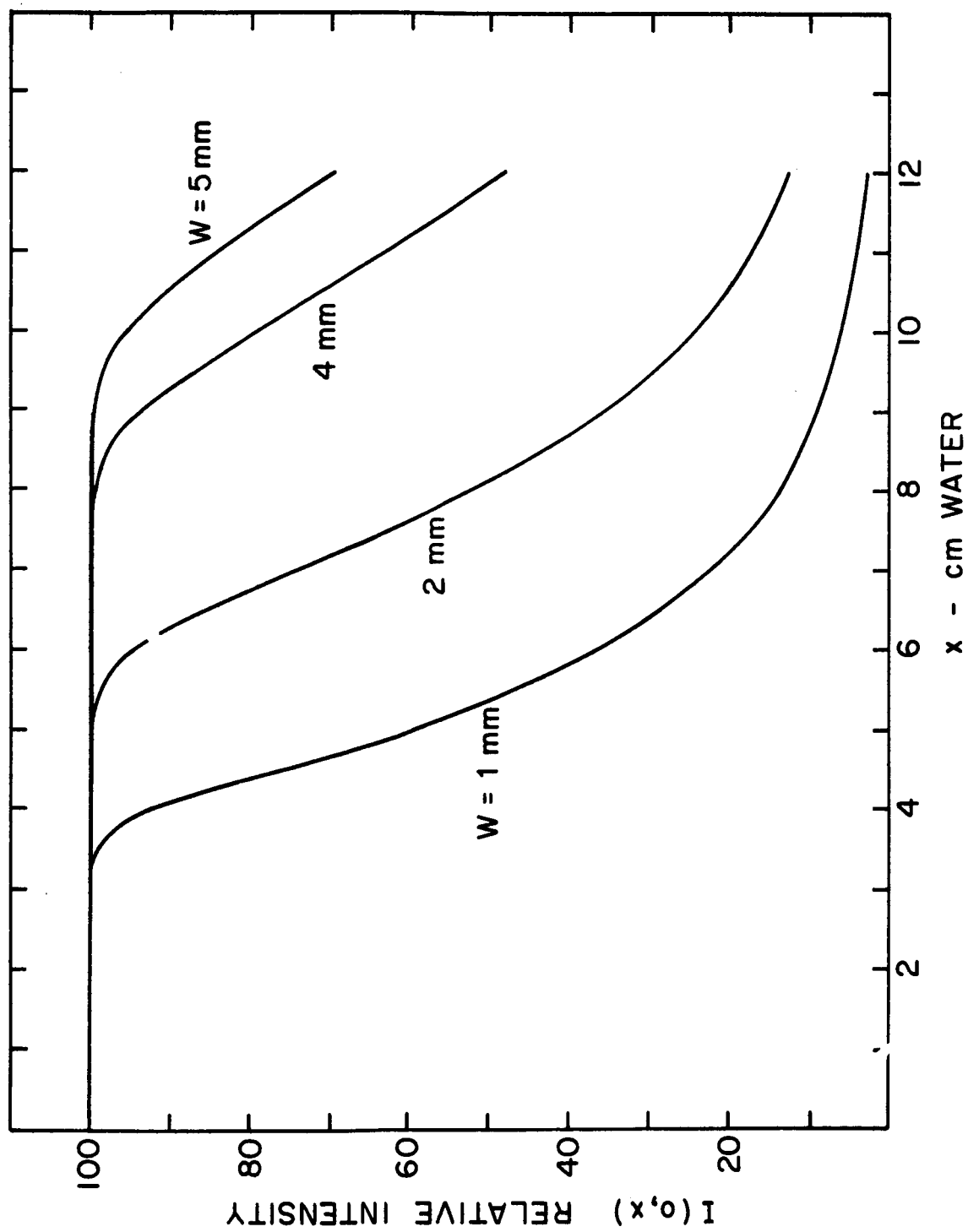
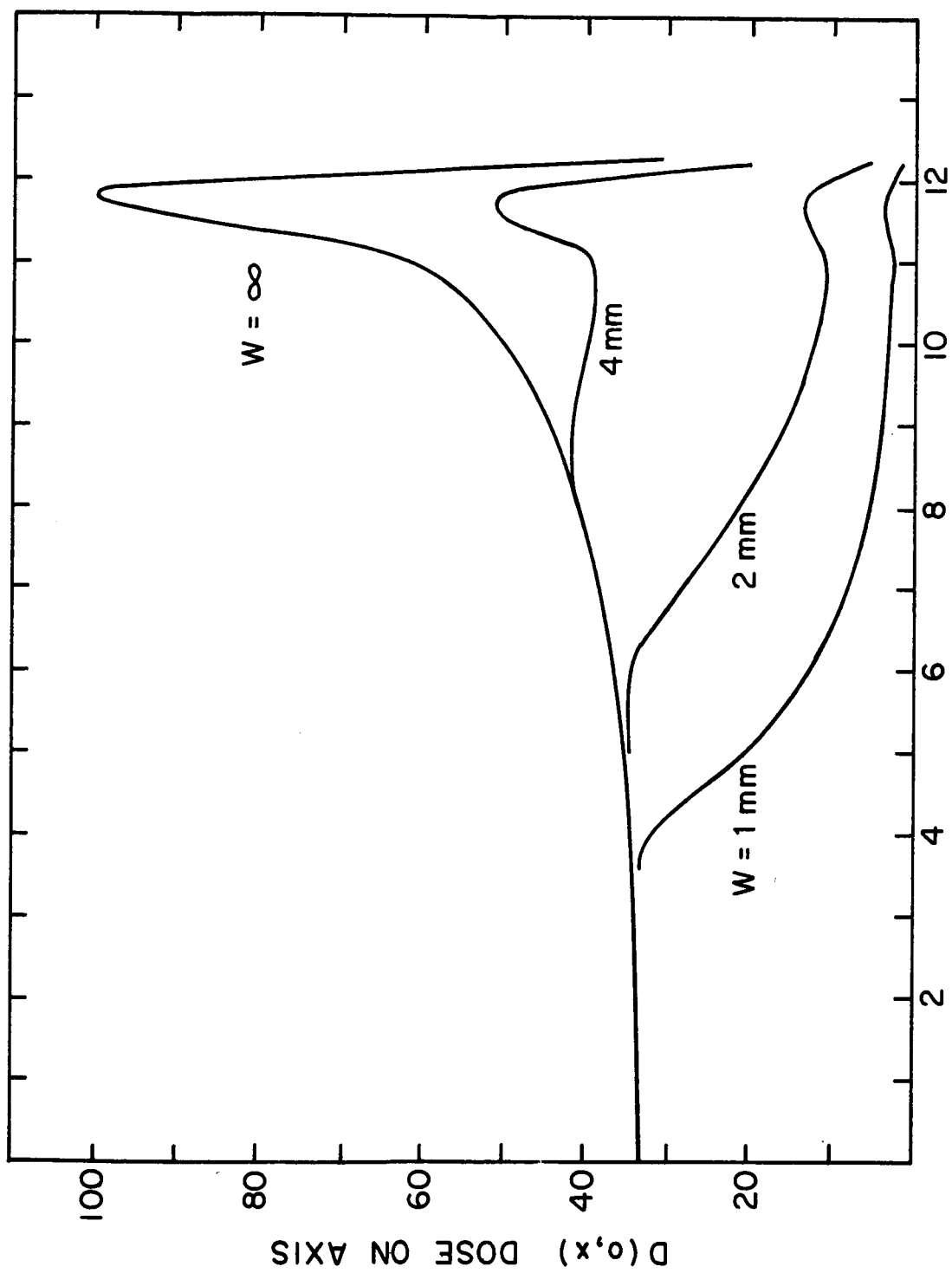


FIGURE 10



x - cm WATER

FIGURE II

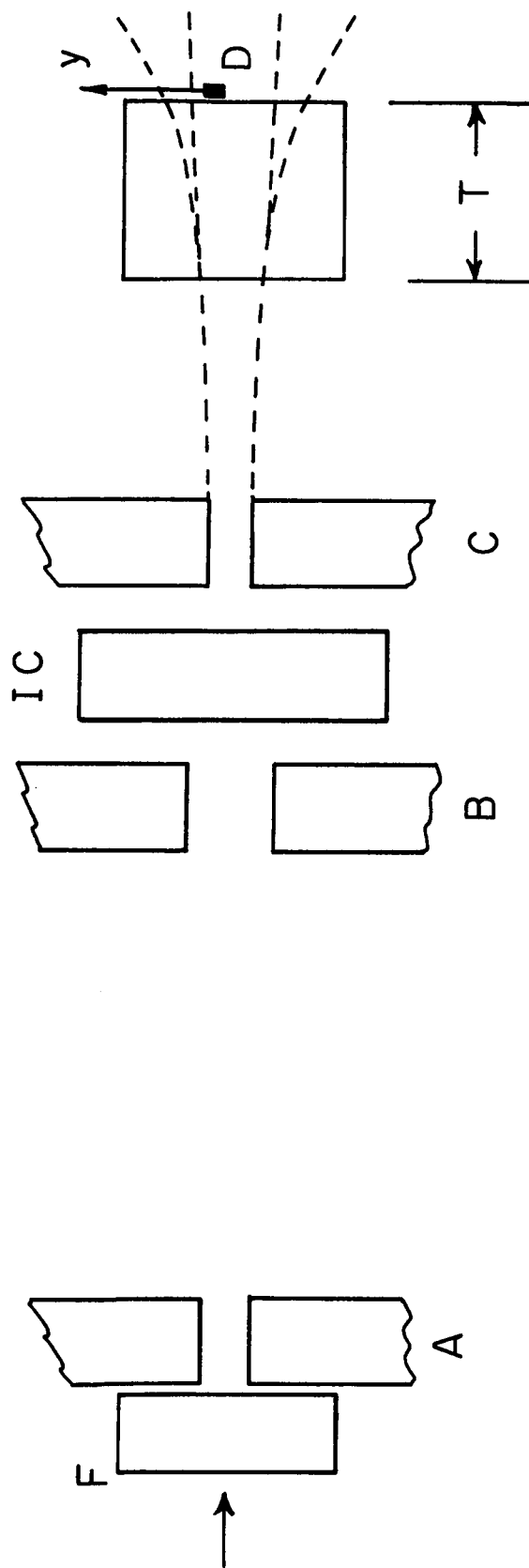


FIGURE 12

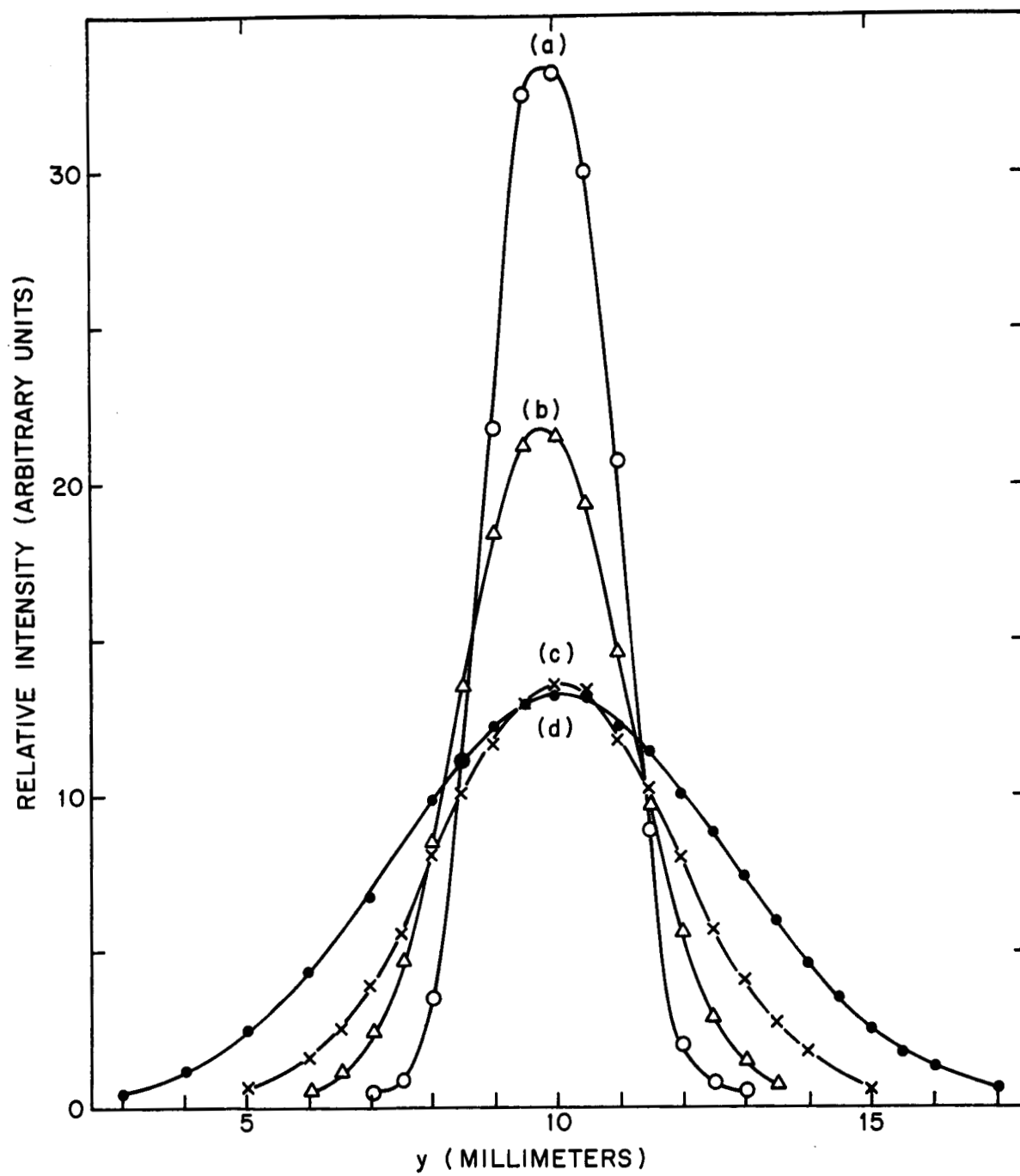


FIG. 13

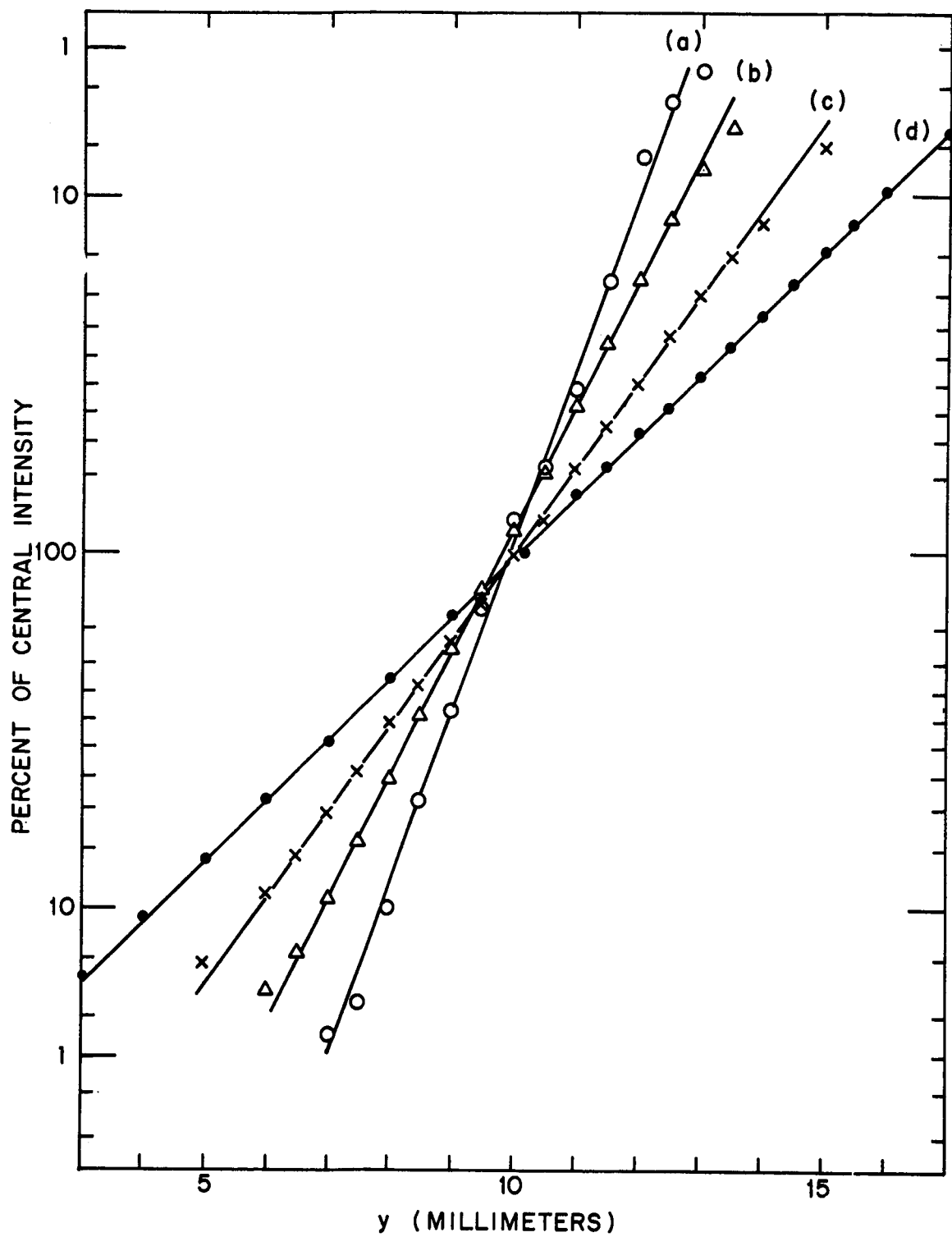


FIG. 14

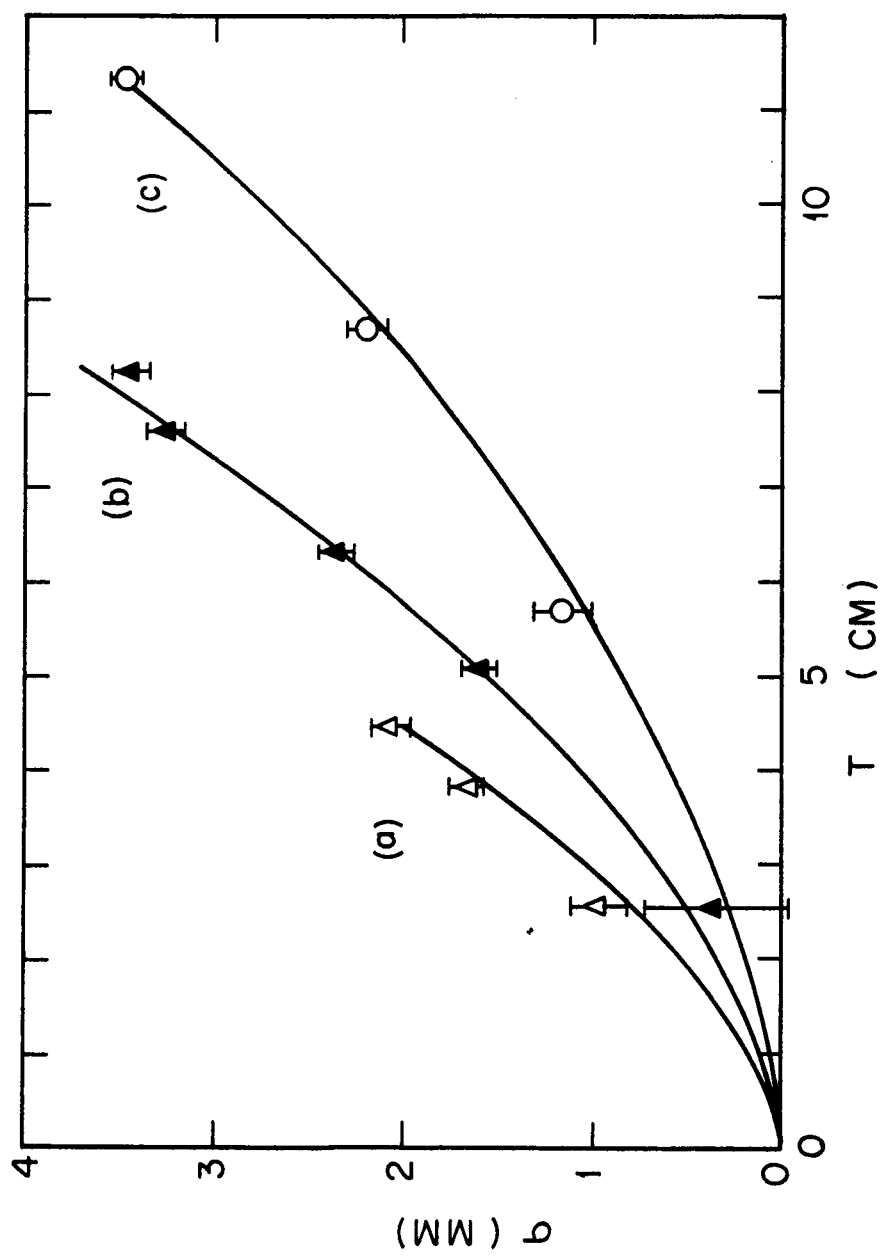


FIGURE 15

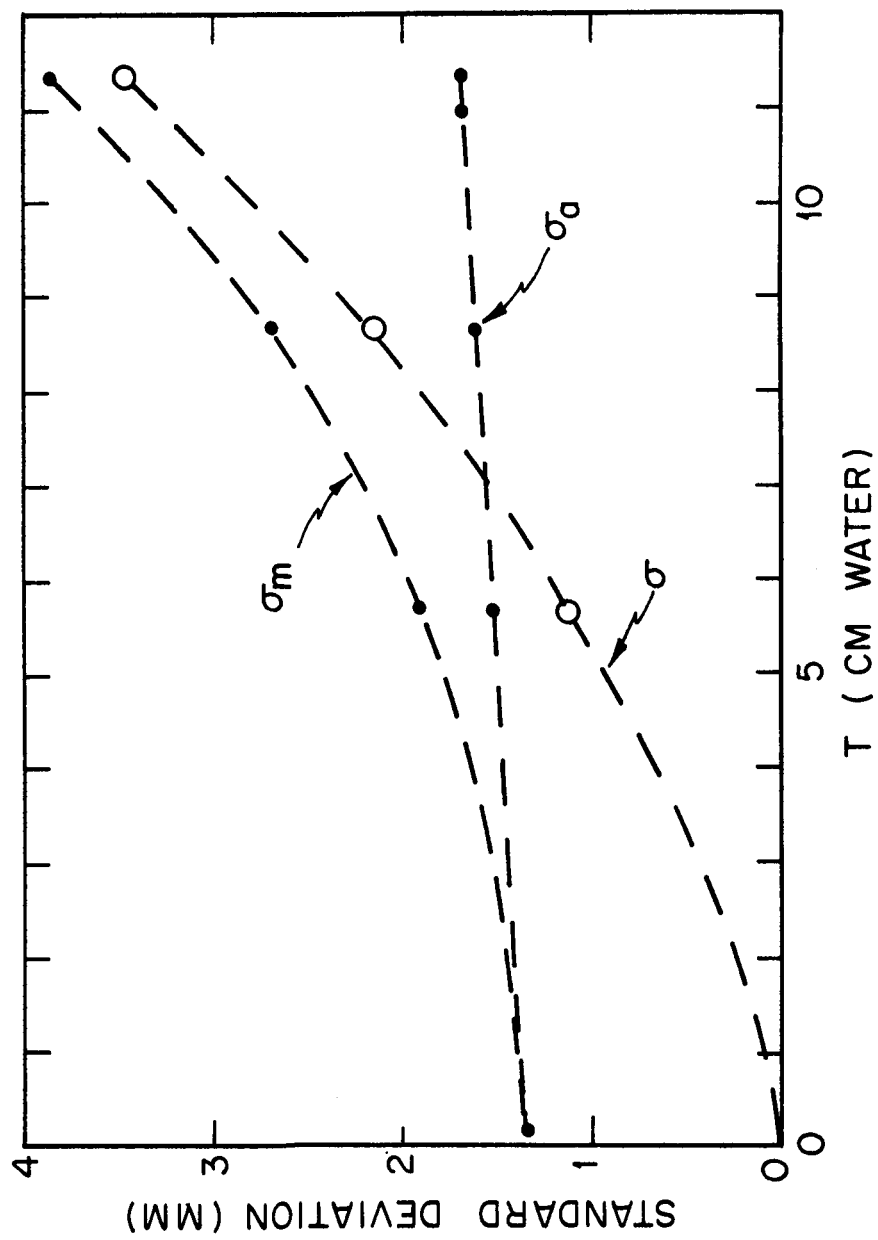


FIGURE 16

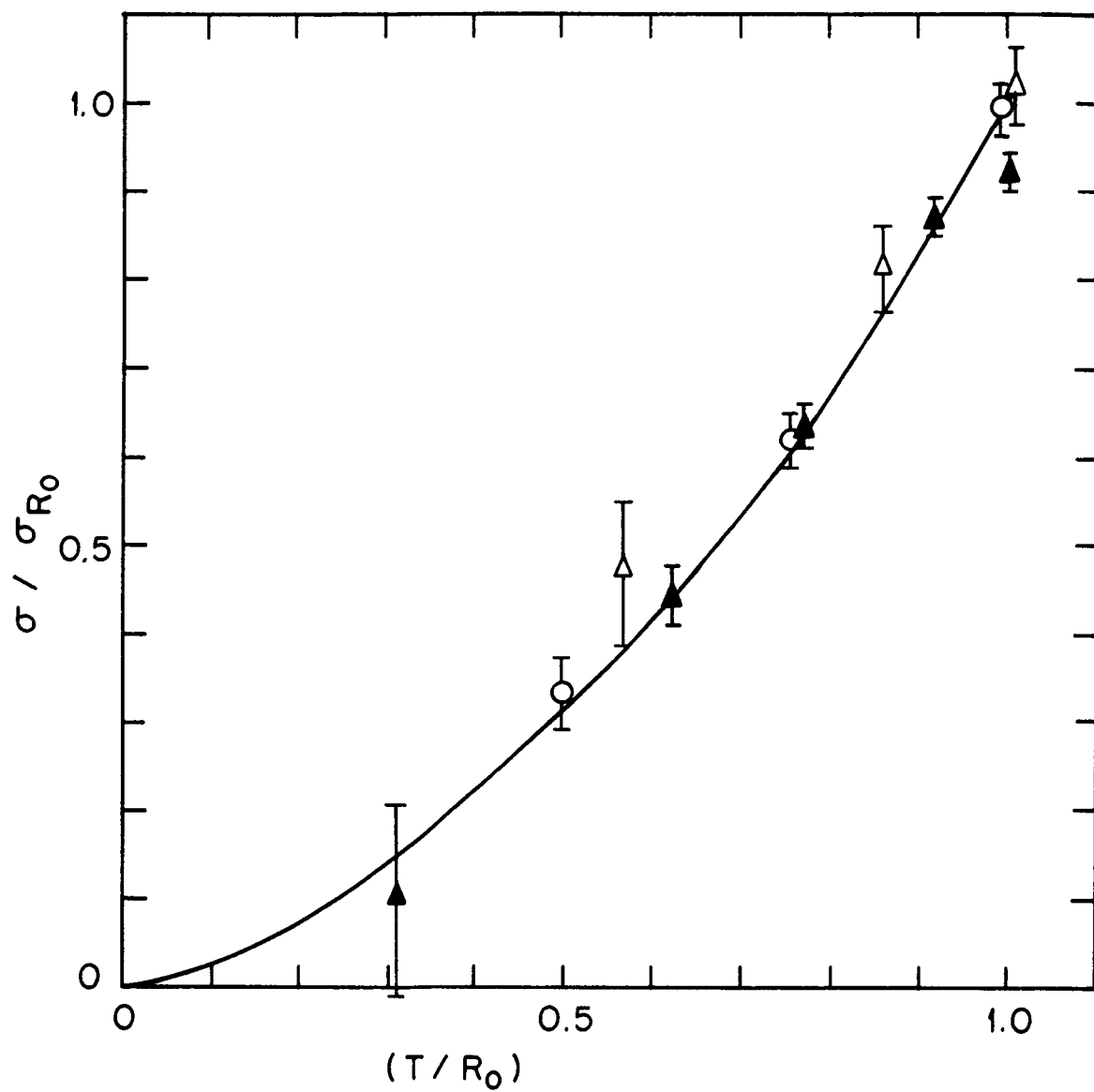


FIGURE 17